Synsint Research Group

Available online at www.synsint.com

Synthesis and Sintering

ISSN 2564-0186 (Print), **ISSN** 2564-0194 (Online)

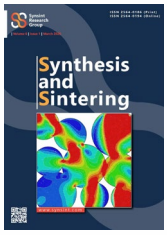

Research article

Green synthesis of Cr_2O_3 nanopigments via bioremediation of chromic acid using Convolvulus arvensis L. extract

Shanli Salahi [a,*], **Mohammad Reza Mobedi** [b]

[a] *Department of Metallurgical and Materials Engineering, Gazi University, Ankara, Türkiye*
[b] *Avizhe Bespar Nazhu Company, East Azarbaijan, Iran*

A B S T R A C T

The rapid growth of industrialization has greatly increased water pollution, and without necessary precautions, serious environmental and public health risks have emerged. In the initial stage, contaminated water samples containing chromic acid, a known carcinogen, were purified using the herbal extract of Convolvulus arvensis L. The obtained extract served as a bioremediation agent, enabling effective removal of chromic acid. After filtration, hexavalent chromium ions (Cr(VI)) were reduced to trivalent chromium ions (Cr(III)), and the resulting precipitate was transformed into chromium(III) oxide (Cr_2O_3) nanopigments through further processing. The removal efficiency was evaluated through detailed analyses using a Hach DR900 spectrophotometer, confirming that the target contaminant was removed to nearly 100%, indicating almost complete elimination. Further characterization of the synthesized Cr_2O_3 nanopigments was performed using Scanning electron microscopy (SEM), X-ray diffraction (XRD), Fourier transform infrared spectroscopy (FTIR), and ultraviolet-visible (UV-Vis) spectroscopy. These comprehensive analyses verified both the successful synthesis and the structural integrity of the nanoparticles. The results support the effective use of plant extracts for the bioremediation of toxic Cr heavy metal ions and demonstrate the practicality of this method for nanoparticle production. The Cr_2O_3 nanopigments with diameters ranging from approximately 10 to 30 nanometers were successfully synthesized and exhibited spherical and polygonal morphologies, with approximately 96% chromium purity.

KEYWORDS

Industrial heavy metal pollution
Carcinogen
Chromic acid
Cr_2O_3 nanopigments
Bioremediation

OPEN ACCESS

1. Introduction

The accelerating pace of industrial growth has significantly intensified environmental pollution, with heavy metals emerging as a special class of pollutants. These metals, often by-products of industrial processes, pose significant risks due to their widespread distribution and harmful effects on ecological and human health [1]. Chromium has been classified by the United States Environmental Protection Agency (EPA) as a highly hazardous substance and categorized as a Group A human carcinogen due to its pronounced toxic effects [2]. Although natural processes can contribute to chromium release, industrial emissions are the primary source of environmental pollution. The recent escalation in chromium demand is closely linked to the rapid industrialization of developing countries, which has significantly increased global use. As a result, anthropogenic chromium is increasingly discharged into the environment [3]. Excessive chromium concentration is primarily attributable to industrial activities such as stainless steel manufacturing, chromium and chromate production and plating, pigment synthesis, leather tanning, textile manufacturing effluents, and fuel combustion (coal, natural gas, and oil), with additional contributions from welding, polishing, and grinding [4, 5].

* Corresponding author. *E-mail address:* shanli.salahi@gmail.com (S. Salahi)
Received 8 January 2026; Received in revised form 13 March 2026; Accepted 13 March 2026.

https://doi.org/10.53063/synsint.2026.61325

Chromium is a widespread marine pollutant, and its presence in seawater contaminates marine flora and fauna, which subsequently enter the human food supply. This element is distributed across environmental matrices, including atmospheric, aquatic, terrestrial, and alimentary systems. The dominant exposure pathway for chromium is inhalation of contaminated air, with additional potential routes including oral intake of chromium-contaminated water and food and direct dermal contact with chromium-containing products [6]. The vigorous carcinogenic properties of chromates, especially those of sodium, strontium, potassium, and calcium, as well as all soluble Cr(VI) compounds, have been widely recognized to significantly increase the risk of cancer among workers exposed to these in industrial workplaces [7, 8].

Chromium primarily exists in two oxidation states: trivalent (Cr^{3+}) and hexavalent (Cr^{6+}). The trivalent form is less hazardous, as it tends to precipitate as insoluble compounds in aqueous systems. In contrast, hexavalent chromium, characterized by a higher oxidation state, exhibits pronounced toxicity and carcinogenicity due to its high water solubility and stability under various environmental conditions. This inherent risk requires significant efforts to develop and implement effective removal strategies for Cr^{6+}. As a result, various methodologies for reducing hexavalent chromium pollution in drinking water sources have been extensively studied within the framework of regulatory standards of many countries, which set the permissible limits in the range of 0.05 to 0.1 ppm [9–11]. These studies are essential in light of the growing environmental and public health sensitivity worldwide. It is important to note that Cr(III) compounds have approximately 100 times lower toxicity than Cr(VI) [12], underscoring the critical importance of the present research. Although Cr(VI) and Cr(III) are classified as genotoxic, their toxicological effects differ significantly in their underlying molecular mechanisms. These differences suggest that Cr(VI) poses greater environmental and health risks due to its higher reactivity and bioavailability.

Cr(VI) compounds enter cells via sulfate anion channels and are rapidly reduced intracellularly by reducing agents such as glutathione (GSH) and ascorbate. This process converts Cr(VI) into highly reactive Cr(V) and Cr(IV) intermediates, which are ultimately reduced to Cr(III) compounds [13–15]. In this process, molecular oxygen is activated and reduced to produce the superoxide anion ($\cdot O_2$), which is then converted to hydrogen peroxide (H_2O_2) via a reaction that initiates mutagenesis. The intermediates formed react with H_2O_2, thereby generating various reactive oxygen species (ROS) via the Fenton reaction. These ROS include superoxide, hydrogen peroxide, singlet oxygen, and hydroxyl radicals, and their presence damages cellular components, contributing to genotoxicity and cellular stress [14–17]. Excessive accumulation of these reactive intermediate species can lead to oxidative stress, which disrupts cellular homeostasis and causes serious DNA damage, such as DNA-protein crosslinks (DPCs), DNA strand breaks, and Cr-DNA adducts. These structural disruptions compromise the integrity of genetic material and destabilize cellular mutations and their progression, further aggravating mutagenic effects. Thus, such damage can profoundly affect cellular genetic stability, potentially triggering carcinogenic transformations [18, 19]. In this context, the International Agency for Research on Cancer (IARC) has classified Cr(VI) as a substance with a proven human carcinogenic effect and included it in the list of Group I carcinogens [20, 21]. Exposure to Cr(VI) compounds significantly increases the risk of respiratory tract cancers in occupational settings [20, 22]. Simultaneously, Cr(VI) has the potential to exert its carcinogenic effects on additional internal organs, particularly within the gastrointestinal tract [23, 24].

Hexavalent chromium ions, manifesting primarily as chromate (CrO_4^{2-}) and dichromate ($Cr_2O_7^{2-}$), are widely used in various industrial applications, including electroplating, leather tanning, wood preservation, and textile production. To date, several methods have been used to remove Cr^{6+}, including ion exchange, reverse osmosis, biological treatment, and carbon filtration. In order to eliminate chromium ions, sulfuric acid has frequently been combined with either iron (II) sulfate or sodium metabisulfite. The first method results in significant sludge production and increased chemical use, posing environmental and economic challenges. The second method, although proven effective, finds more limited use due to the high cost of raw materials and the difficulty of safely handling and disposing of the toxic and pungent sulfur dioxide (SO_2) gas produced during the process. Since the production of this gas poses serious environmental and health risks, the frequency of this method is decreasing [25, 26]. Recently, researchers have shown increasing interest in green and biological methods for removing industrial pollutants. These methods stand out as a very promising alternative to traditional treatment technologies due to their low cost, high efficiency, prevention of toxic chemical waste formation, and easy access to a wide range of biomaterials. These innovative approaches can make significant contributions to achieving environmental sustainability goals [27, 28].

Plant extracts that gain regenerative properties with the presence of alkyl, phenolic, and aldehyde groups play a critical role in chromium filtration processes. In this approach, Cr(VI) is first reduced to Cr(III) using a reducing agent, and then precipitated as chromium(III) hydroxide by increasing the pH. The aqueous extract from the plant Convolvulus arvensis L. stands out as a particularly effective biomaterial for accelerating and improving the efficiency of these reduction and precipitation processes [29].

The Convolvulaceae family, commonly known as the morning glory family, comprises approximately 1,880 species distributed across 57 genera within the order Solanales. Members of the Convolvulaceae family are distributed globally, except in circumpolar regions [30, 31]. The genus Convolvulus (from Latin convolere), belonging to the Convolvulaceae family (commonly known as the bindweed or glory family), comprises approximately 250 species of flowering plants. This family is of significant medicinal and economic importance, encompassing a variety of growth forms, including trees, shrubs, and herbs [32, 33]. The taxonomic classification of Convolvulus species, encompassing both common and Latin names, has historically been complicated by their widespread global distribution. This complexity persisted until the adoption of universally accepted nomenclature standards [34]. The Convolvulus genus exhibits a remarkable diversity of species predominantly in the regions of Western and Central Asia, Macaronesia, the Mediterranean basin, the Arabian Peninsula, and East Africa [35]. The scientific community has increasingly investigated Convolvulus species, particularly their extracts and oils, due to their significant phytochemical compositions, high bioavailability, potency, and safety profiles [32]. Convolvulus arvensis L., commonly known as field bindweed, is recognized as one of the most common species in the same genus [36] and characterized by rich and complex chemical constituents such as flavonoids, sterols, triterpenes, tannins, cardiac glycosides, coumarins, saponins, alkaloids, and phlorotannins [37].

Recent advances in nanoscience have enabled nanopigments to be widely used across many industrial sectors, including ceramics, coatings, glass, and polymers. These nanopigments offer significant benefits in industrial applications due to their superior stability and performance. Synthesized nanopigments contribute to the development of long-lasting and more effective materials by improving the performance and durability of the products to which they are applied. These developments increase the quality standards of industrial products while also providing environmental and economic benefits [38]. Cr_2O_3 stands out for its unique properties, including high pigment opacity, excellent UV light attenuation, resistance to degradation, and visible light transmittance. These qualities have enabled Cr_2O_3 to find a wide range of uses in various industrial applications, such as construction materials, refractories, ceramic glazes, paints, and plastics [39, 40]. The versatility of chromium(III) oxide stems from its superior physicochemical properties, such as exceptional oxidation resistance and a high melting point [41]. In particular, the permanent green hue in cement- and lime-based building materials can be obtained by adding Cr_2O_3 [40]. In addition, the use of nanosized chromium(III) oxide pigments has enabled new and advanced functionalities in surface coating technologies. Pigments reduced to nanometric dimensions exhibit superior performance compared to traditional pigments, owing to their higher surface area and improved dispersion properties. These developments increase the UV resistance, chemical resistance, and long-term stability of coatings, while also enabling more uniform color distribution and smoother surfaces. These advantages of nano-chromium oxides offer great potential, especially for high-performance industrial paints, automotive coatings, and advanced decorative applications [42, 43].

The need to reduce the adverse environmental and health effects of industrial wastewater pollution has driven research into innovative remediation strategies. This study aims to add a new dimension to current approaches in this field by introducing a pioneering bioremediation method using Convolvulus arvensis L. extract. This method effectively reduces carcinogenic chromic acid to synthesize Cr_2O_3 nanopigments, which were shown to provide almost complete removal efficiency by Hach DR900 spectrophotometric analysis. The use of Convolvulus arvensis L., a cost-effective and widely available botanical resource, offers a practical and sustainable solution in this process, making an important contribution to eliminating industrial wastewater pollution. Compared to traditional methods, this approach stands out as an exemplary "green" technology by exhibiting greater economic efficiency, ease of application, and environmental sustainability. Furthermore, this study aims to evaluate the potential industrial applications of synthesized nanopigments in textile dyeing, ink formulation, and ceramic glazing.

2. Materials and methods

2.1. Extraction of Convolvulus arvensis L. herb

The preparation of the herbal extract from Convolvulus arvensis L. started with harvesting fresh leaves and stems, which were then washed with distilled water to remove contaminants. The cleaned plant material was air-dried at room temperature until completely moisture-free. After drying, about 20 g of Convolvulus arvensis L. were placed in a beaker with 200 ml of distilled water. The mixture was boiled and simmered for 15 minutes to thoroughly extract bioactive compounds. Once cooled, the liquid extract was filtered through Whatman No. 40 filter paper to remove any remaining solids. The filtrate was stored at 3 °C for subsequent use.

2.2. Preparation of natural and artificial effluent of chromic acid

Natural chromic acid effluent samples were collected from a chromium plating facility on both high- and low-production days to capture a representative range of industrial wastewater conditions. The samples were stored at 3 °C under controlled conditions until analysis to maintain their original chemical properties. Concurrently, a synthetic chromic acid effluent was prepared by dissolving chromium(IV) oxide in distilled water, yielding concentrations of 2000, 4000, and 6000 ppm, corresponding to 2, 4, and 6 g of chromium(IV) oxide per liter. This method was selected to facilitate a systematic investigation of the physicochemical properties of the chromic acid effluent and to ensure consistent experimental conditions.

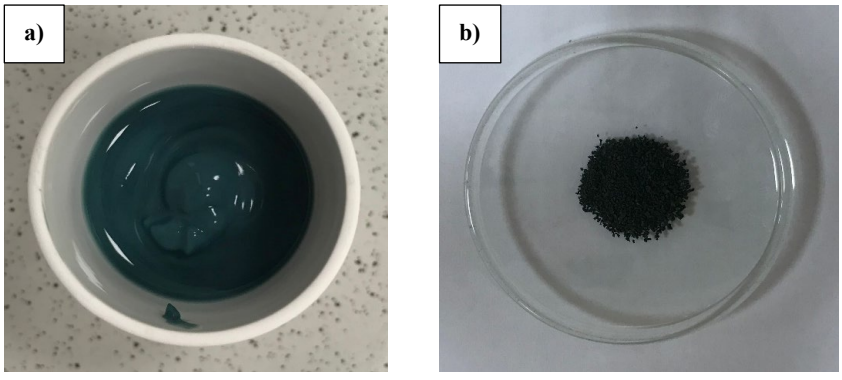

Fig. 1. a) Colloidal and b) powdered form of synthesized Cr_2O_3 nanopigments.

2.3. Investigation of chromium elimination from industrial wastewater

The study on chromium removal from contaminated samples used a systematic approach to evaluate the effectiveness of different treatment methods. In the first stage, five samples were prepared, each with a volume of 50 ml. 1 ml of 32% hydrochloric acid (Merck, 100319) and 50 ml of plant extract solution were added to each sample. Acid was added to promote the reduction of Cr(VI) ions (chromate and dichromate) to Cr(III) form in an acidic medium. The prepared samples were kept at room temperature for 24 hours to complete the reaction. At the end of this period, the concentration of Cr(VI) ions in the samples was measured using a Hach DR900 spectrophotometer to evaluate the removal efficiency.

2.4. Synthesis of Cr_2O_3 nanopigments

To synthesize Cr_2O_3 nanoparticles, a 1 M sodium hydroxide solution was prepared by dissolving 40 g of flake sodium hydroxide (Sigma Aldrich, Germany) in 1 liter of distilled water. Subsequently, 5 ml of a polyvinylpyrrolidone (PVP) solution was combined with 200 ml of a Cr(III) ion solution, and the mixture was stirred magnetically. Sodium hydroxide solution was then added dropwise to the mixture to adjust the pH to 9. The resulting nanoparticles were separated through filtration using Whatman No. 40 filter paper. Following filtration, the nanoparticles were washed twice with distilled water and once with pure acetone (Merck, Germany) to remove any residual impurities. Finally, the washed nanoparticles were calcined at 600 °C for 90 minutes to achieve the desired crystallinity and phase purity.

3. Results and discussion

3.1. Filtration efficiency

In this research, the primary aim was to remediate carcinogenic chromic acid from industrially polluted aqueous systems using Convolvulus arvensis L. herb extract. The prepared plant extract was used to facilitate chromium extraction from contaminated water. Subsequently, the extracted chromium was subjected to a transformation process to synthesize Cr_2O_3 nanopigments, thereby enabling the transformation of hazardous chromium into more controllable nanomaterials. The filtration efficiency results for carcinogenic chromic acid, as detailed in Table 1, indicate an exceptionally high level of contaminant removal, achieving near-complete elimination with a virtually complete efficacy.

Upon adding the Cr(III) ion solution obtained from the filtration process of industrial waste to the synthesis of nanoparticles, a notable and progressive change in the solution's color was observed. This transition, from the initial state to a recognizable bright rust-green hue, occurs when the solution pH reaches 9 and serves as a clear indicator of the successful synthesis of Cr_2O_3 nanopigments.

3.2. Microstructural characterization

The synthesized Cr_2O_3 nanoparticles were analyzed by SEM for comprehensive morphological and dimensional characterization, as depicted in Fig. 3. SEM micrographs revealed a distinct spherical-polygonal morphology, indicating the crystalline structure formed under controlled synthesis conditions. Such morphological homogeneity demonstrates that the nucleation and growth dynamics during the synthesis process have been meticulously optimized. The consistency in the shape and size of the synthesized nanoparticles is critical, especially for targeted applications, since these features directly determine physicochemical characteristics.

The elemental composition of the synthesized Cr_2O_3 nanopigments was characterized in detail using EDS analysis, with the data presented in Fig. 4.

The EDS spectrum clearly reveals chromium (Cr) and oxygen (O) as the main components, indicating that no significant impurities were detected. The weight percentages of the elements obtained as a result of the analysis were determined as 95.8% for Cr and 4.2% for O, and the associated uncertainty (σ) for both elements was recorded as 0.2%. The findings reveal the stoichiometric Cr/O ratio, consistent with the expected theoretical composition of Cr_2O_3 (Cr: 68.42%, O: 31.58% atomic percentage), along with the apparent dominance of Cr peaks in

Table 1. Pre-filtration and post-filtration concentration of Cr^{6+} ions (ppm) in wastewater samples.

Sample	Concentration of CrO_3 (ppm)	Pre-filtration concentration of Cr^{6+} (ppm)	Post-filtration concentration of Cr^{6+} (ppm)
Simulated effluent			
1	2000	1039	0.01
2	4000	2078	0.07
3	6000	3117	0.10
Natural effluent			
4	**Low-Cr concentration days**	883.9	0.01
	1700		
5	**High-Cr concentration days**	2547	0.09
	4900		

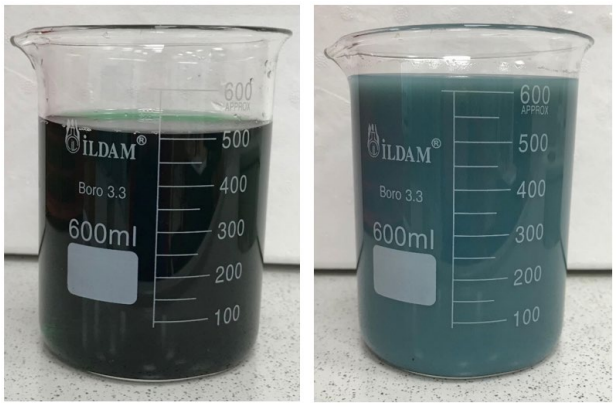

Before The Synthesis of Cr_2O_3 Nano-pigments ***After The Synthesis of Cr_2O_3 Nano-pigments***

Fig. 2. Synthesis of Cr_2O_3 nanopigments facilitated under alkaline conditions at pH 9.

the spectrum, confirming the successful synthesis of Cr_2O_3 nanoparticles. The slight deviation in oxygen content indicates the presence of surface hydroxyl groups or surface-bound oxygen forms, which are frequently observed due to the high surface area and reactivity characteristics of oxides at the nanometer scale. The absence of extraneous elemental peaks proves that the synthesized nanopigments are highly pure, making them suitable for applications requiring rigorous material specifications, such as advanced pigments and coating processes.

The particle size distribution of Cr_2O_3 nanopigments was analyzed in detail, as shown in the histogram in Fig. 5. A Gaussian distribution was used to characterize the statistical dispersion of particle dimensions. The particle diameter ranges from 10 nm to 30 nm, with a clear unimodal distribution. The central tendency of the particle size is determined by the mean diameter (μ) of 18.16 nm, which represents the average particle size within the sample. The relatively low standard deviation (σ) of 3.65 nm highlights the narrow distribution. It indicates a high degree of uniformity in particle size, which is a critical factor in applications where size consistency is essential for performance.

The histogram shows a gradual increase in frequency starting at 10 nm, a sharp peak around 18 nm, and then a gradual decrease towards larger diameters. This distribution is slightly skewed to the right, likely due to a small aggregation of larger particles formed during the synthesis procedure. The presence of this slight skewness indicates that, while most particles are near the mean size, a small subset has larger diameters, potentially due to variations in nucleation and growth rates during synthesis. The precise clustering of particle sizes around the mean reveals that the synthesis method effectively controls nucleation and growth, yielding a uniform product. The relatively narrow size distribution and the predominance of particles near the average diameter indicate an optimized synthesis process, which is crucial for maintaining nanoparticle stability in subsequent applications.

3.3. Structural analysis

The XRD profile of Cr_2O_3 nanopigments is shown in Fig. 6. Furthermore, the analysis of these XRD patterns was conducted by referencing the ICDD 00-051-0959 and 00-059-0308 PDF cards data, enabling a comprehensive investigation of the nanoparticles' properties through peak positions (2θ), peak intensities, and full-width at half maximums (FWHM, β). The XRD pattern of the synthesized Cr_2O_3 nanopigments reveals the critical structural characteristics, indicating

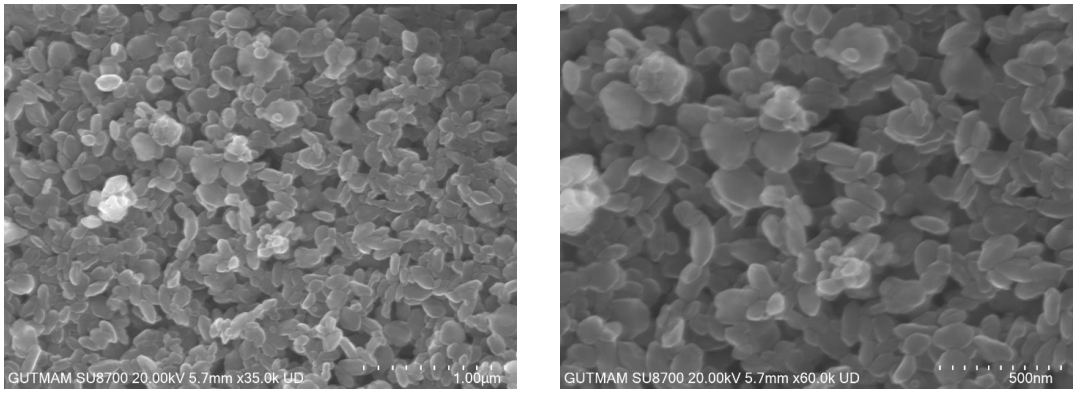

Fig. 3. SEM micrographs of synthesized Cr_2O_3 nanopigments.

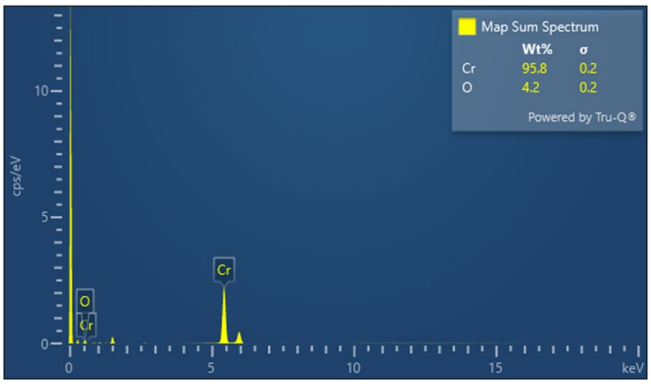

Fig. 4. Comprehensive elemental analysis of synthesized Cr_2O_3 nanopigments.

the crystalline phases present in the sample. The principal diffraction peaks are detected at 2θ angles approximately at 24.72°, 33.91°, 36.53°, 41.87°, 50.70°, 55.38°, 64.09°, and 65.76°, corresponding to the (012), (104), (110), (113), (024), (116), (214), and (300) crystallographic planes, respectively, characteristic of the rhombohedral α-Cr_2O_3 phase. The most prominent peak at 36.53° aligns with the (110) plane, indicating the crystal structure of Cr_2O_3 nanopigments. The sharp, well-defined peaks reflect the high crystallinity of the synthesized nanoparticles.

The broadening of these peaks indicates the nanoscale dimensions of the crystals, and the Scherrer equation is used to estimate the crystal size from the FWHM of the dominant diffraction peaks. Crystallite sizes were accurately calculated utilizing Scherrer's equation, as specified in Eq. 1 [44].

$$d = \frac{K\lambda}{\beta \cos\theta} \quad (1)$$

where K represents the shape factor (typically 0.9 for spherical particles), λ denotes the X-ray wavelength (CuKα, 1.5406 Å), β is the FWHM of the diffraction peak, and θ is the Bragg angle.

The crystallite size, derived from the FWHM of the most intense diffraction peak corresponding to the (110) plane at 36.53°, indicates that the synthesized Cr_2O_3 nanopigments exhibit a mean crystallite size of approximately 36.29 nm, affirming their nanometric scale and confirming their finely dispersed crystalline nature.

Furthermore, lattice parameters refined using the XRD data reveal that the rhombohedral unit cell of Cr_2O_3 is characterized by lattice constants a = 4.915 Å and c = 13.473 Å. The unit cell volume, calculated from the lattice parameters, is approximately 281.87 $Å^3$, which aligns with the standard reference values. The XRD analysis conclusively demonstrates the successful synthesis of α-Cr_2O_3 nanopigments with a rhombohedral crystal structure. The high degree of crystallinity and the absence of secondary phases or impurities in the XRD pattern indicate that the synthesis process, including the thermal decomposition of precursor materials, is extremely efficient in producing Cr_2O_3 nanoparticles with a pure phase. This detailed structural analysis confirms the integrity and purity of the synthesized Cr_2O_3 nanopigments, rendering them suitable for applications where high crystallinity and phase purity are critical.

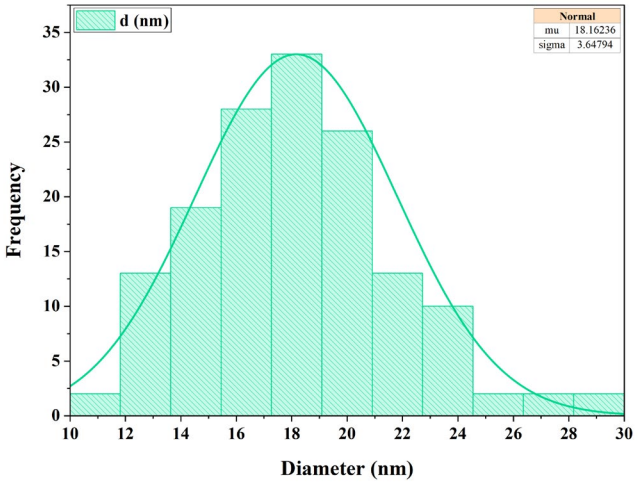

Fig. 5. Size distribution curve of synthesized Cr_2O_3 nanopigments.

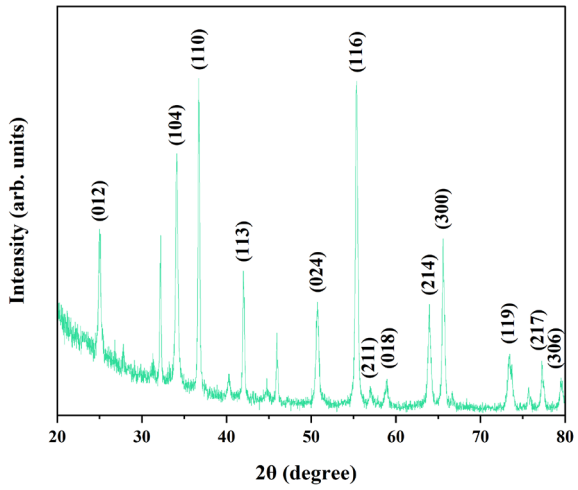

Fig. 6. XRD diagram of Cr_2O_3 nanopigments.

3.4. Optical characterization

The FTIR spectrum of the synthesized Cr_2O_3 nanoparticles exhibits multiple absorption bands. It provides deep insight into the distinct functional groups, complex molecular structure, vibrational modes, and the nuanced bonding interactions characterized within the nanomaterial, as illustrated in Fig. 7.

A broad absorption band at 3448 cm^{-1} corresponds to the O – H stretching vibration, which is usually attributed to hydroxyl groups, possibly due to moisture adsorbed on the nanoparticle surface or residual water from the synthesis process. The width of this band indicates hydrogen bonding interactions. The absorption band at 1616 cm^{-1} corresponds to the bending vibrations of the O–H group [45], further confirming the presence of water or hydroxyl groups on the surface of the nanoparticles.

Typically, metal oxides exhibit distinct absorption bands at wavenumbers below 1000 cm^{-1}, which are mainly attributed to the vibrational dynamics between interatomic bonds. The observed bands in the range of 885 cm^{-1} are attributed to stretching vibrations of Cr=O [46], which indicate the partial oxidation of chromium species or the presence of Cr = O bonds, which is probably due to the moderate oxidation state of chromium within the nanoparticle structure. The sharp absorption bands at 609 cm^{-1} and 532 cm^{-1} are characteristic of Cr–O bond-stretching modes [47, 48], which are fundamental to the α-Cr_2O_3 lattice structure and are consistent with the typical vibrational modes of the Cr–O bonds in crystalline Cr_2O_3. The absorption band at 405 cm^{-1} is particularly noteworthy, as it validates the presence of the semi-crystalline phase in the synthesized Cr_2O_3 nanoparticles [49, 50], which is associated with lattice vibrations of the Cr_2O_3 nanostructure, thereby confirming the semi-crystalline nature of the nanomaterial. Therefore, the FTIR spectra provide important insights into the structural and compositional features of the synthesized Cr_2O_3 nanopigments, highlighting successful synthesis with well-

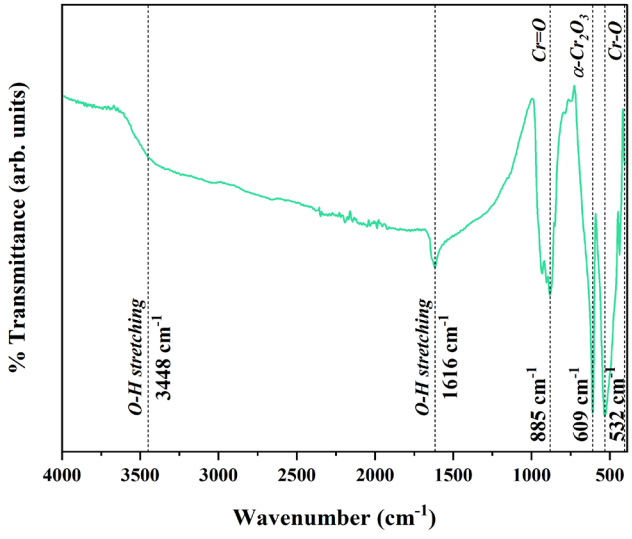

Fig. 7. FTIR spectral curve of Cr_2O_3 nanopigments.

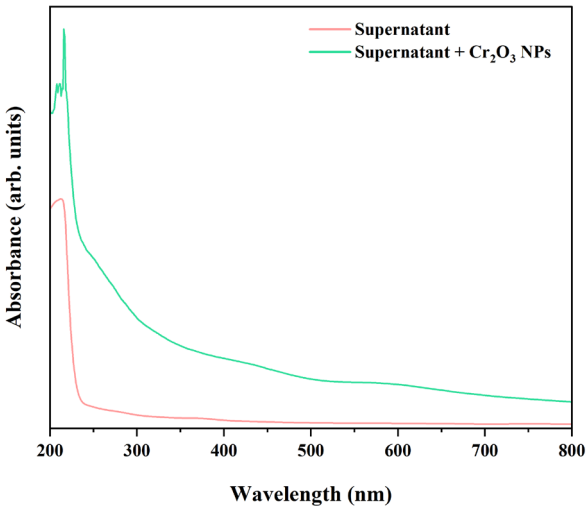

Fig. 8. UV-Vis absorption spectra of the supernatant and the supernatant containing synthesized Cr_2O_3 nanoparticles (NPs) recorded across the wavelength range of 200–800 nm.

defined crystalline properties and revealing surface interactions with moisture and organic residues commonly found on synthesized nanoparticles.

The UV-Vis absorption spectra of the supernatant, both in the presence and absence of the synthesized Cr_2O_3 nanopigments, were accurately recorded in the wavelength range of 200–800 nm and illustrated distinct optical characteristics, as delineated in Fig. 8. The absorption spectrum of the pure supernatant (without Cr_2O_3 NPs) shows a primary absorption peak around 200–300 nm, indicating the presence of residual organic compounds or unreacted precursors in the solution. At the same time, the low absorbance values observed beyond 300 nm indicate minimal light interaction in this region.

In contrast, the spectrum of the supernatant containing Cr_2O_3 nanoparticles showed a significant increase in absorbance in the UV region (200–300 nm), characterized by a prominent, broad absorption peak, indicating strong electronic transitions associated with Cr_2O_3 nanoparticles [49]. This broad peak is likely due to the size distribution of the synthesized nanoparticles and to the intrinsic electronic transitions of chromium oxide (Cr−O) within them. In addition, the spectrum of the Cr_2O_3 nanoparticles with higher absorption extended to the visible region of 400−700 nm [49], which is a characteristic feature of the d−d transitions of Cr^{3+} ions within the Cr_2O_3 lattice, indicating a relatively high degree of crystallinity in the nanoparticles. The absence of sharp features in the visible range indicates a homogeneous particle distribution and minimal agglomeration, which favors uniform optical characteristics in potential applications. The observed spectral features match the expected optical properties of Cr_2O_3 nanoparticles, confirming their successful synthesis.

The optical transitions and corresponding band gap energies (E_g) of the synthesized Cr_2O_3 nanopigments were analyzed in detail through the rigorous application of Tauc and Davis-Mott models [51]: $(\alpha h\nu)^2 = A(h\nu - E_g^d)$ and $(\alpha h\nu)^{1/2} = B(h\nu - E_g^i)$ for direct and indirect allowed transitions. In these equations, hν represents the photon energy, while A and B are material-specific constants, and E_g^d and E_g^i denote the direct and indirect band gap energies, respectively. The graphical representation of $(\alpha h\nu)^2$ as a function of $(\alpha h\nu)$ is provided in Fig. 9.

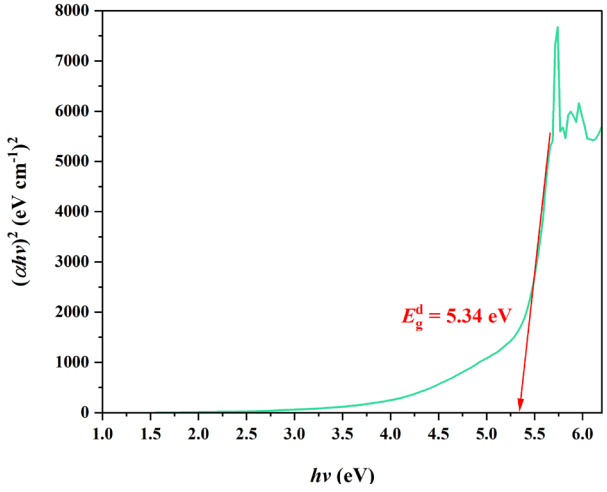

Fig. 9. The direct band gap energy (E_g^d) curve of the Cr_2O_3 nanopigments.

Fig. 10. Schematic representation of a device engineered for the filtration of chromium from industrial wastewater.

The optical band gap energy of Cr_2O_3 nanopigments was calculated to be 5.34 eV using a Tauc plot. This value differs significantly from the band gap range reported in the literature for bulk Cr_2O_3, which has a lower band gap [52, 53]. The increase in band gap energy can be attributed to quantum confinement effects, which relate directly to the nanoscale dimensions of Cr_2O_3 pigments. As particle size decreases, the surface-to-volume ratio increases markedly, resulting in a more pronounced separation of energy levels. This leads to a larger gap between quantized energy levels, expanding the band gap. This phenomenon is explained by the quantum confinement effect, which occurs when the movement of charge carriers, electrons and holes, is restricted to a nanoscale region. As particle size decreases, charge carriers are confined to a smaller volume, leading to energy-level separation. Consequently, a larger energy difference arises, increasing the band gap energy [54]. This is reflected in the steep linear region observed in the Tauc plot, indicating a direct-transition-like optical behavior in the nanoscale Cr_2O_3 system. The shift in electronic structure due to nanocrystallinity allows for band-gap tuning.

The operational methodology of this research project is meticulously explained, with a schematic representation of the filtration apparatus shown in Fig. 10. This specially designed system begins with the transfer of chromium-laden industrial wastewater into the primary holding tank using a plant-derived extract. During this process, Cr^{6+} in the wastewater are converted to less toxic Cr^{3+} through chemical reduction. This reduction procedure minimizes chromium's environmental impacts and improves water purification, underscoring the importance of the filtration process for environmental sustainability.

The solution obtained after the reduction process is transferred to the secondary holding tank, where it is treated with sodium hydroxide solution via syringe. This step ensures the precipitation of Cr^{3+} as chromium(III) hydroxide [$Cr(OH)_3$]. A water pump is used to maintain solution homogeneity and optimize the precipitation process. This mechanical mixing ensures uniform distribution throughout the solution, allowing chromium ions to precipitate effectively and obtain a phase free of the desired impurities. The settled suspension is then transferred to the tertiary holding vessel, where filtration occurs to separate the $Cr(OH)_3$ formed in the solid phase. In this stage, the solid chromium is filtered out. Meanwhile, the waste liquid with significantly reduced chromium content is carefully drained through the outlet at the bottom of the tertiary vessel. This process reduces the environmental impact of the waste liquid and prepares the recovered chromium for further processing stages.

4. Conclusions

The findings of this study reveal the widespread presence of chromic acid in contaminated water and soil, emphasizing its serious, harmful effects on the environment and public health. The carcinogenic nature of chromic acid is well-documented, and its presence in natural environments underscores the urgent need for action, especially given global issues such as water scarcity and ecosystem degradation. Therefore, reducing chromic acid pollution in water and soil is essential for both environmental sustainability and public health protection. Convolvulus arvensis L. extract is highly effective at removing chromic acid from contaminated samples, serving as a cost-effective and readily accessible plant resource. This innovative approach has great potential to address heavy metal pollution by offering a sustainable, practical solution. The study not only demonstrates the effectiveness of plant extracts in reducing the harmful effects of pollutants such as chromic acid but also contributes to growing research on plant-based bioremediation methods. Additionally, it successfully transforms hazardous chromic acid into valuable Cr_2O_3 nanopigments through an environmentally friendly process. These Cr_2O_3 nanoparticles represent a meaningful advancement in environmental sustainability and nanotechnology, with high potential

for a range of industrial applications. Their nano-sized structure and excellent physical properties enable applications in construction materials, textile dyeing, ink formulations, and ceramic glazing, further underscoring the significance of this research. The high purity and precise geometric configurations of the synthesized Cr_2O_3 nanoparticles make them great candidates for meeting advanced technological needs in materials science and industry. In this way, the study offers a solution to a key environmental challenge while paving the way for the sustainable production of valuable nanomaterials from hazardous waste. The successful combination of environmental pollutant removal and nanopigment production presents a promising approach for both environmental improvement and resource recovery.

CRediT authorship contribution statement

Shanli Salahi: Conceptualization, Data curation, Methodology, Investigation, Validation, Visualization, Supervision, Writing – original draft, Writing – review & editing.
Mohammad Reza Mobedi: Conceptualization, Data curation, Methodology, Investigation, Validation, Visualization, Supervision, Writing – original draft, Writing – review & editing.

Data availability

The data underlying this article will be shared on reasonable request to the corresponding author.

Declaration of competing interest

The authors declare no competing interests.

Funding and acknowledgment

The global patent application for the international commercialization of this research study belongs to Avanos Medical Agriculture and Environmental Technologies LTD., located in Ankara, Türkiye.

References

[1] B. Kakavandi, R.R. Kalantary, M. Farzadkia, A.H. Mahvi, A. Esrafili, et al., Enhanced chromium (VI) removal using activated carbon modified by zero valent iron and silver bimetallic nanoparticles, J. Environ. Heal. Sci. Eng. 12 (2014) 115. https://doi.org/10.1186/s40201-014-0115-5.

[2] H. Norouzi, D. Jafari, M. Esfandyari, Study on a new adsorbent for biosorption of cadmium ion from aqueous solution by activated carbon prepared from Ricinus communis, Desalin. Water Treat. 191 (2020) 140–152. https:/doi.org/10.5004/dwt.2020.25702.

[3] J.W. Ran Zhao, B. Wang, Q. Tao Cai, X. Xia Li, M. Liu, et al., Bioremediation of Hexavalent Chromium Pollution by Sporosarcina saromensis M52 Isolated from Offshore Sediments in Xiamen, China, Biomed. Environ. Sci. 29 (2016) 127–136. https://doi.org/10.3967/bes2016.014.

[4] F.H. Khan, K. Ambreen, G. Fatima, S. Kumar, Assessment of health risks with reference to oxidative stress and DNA damage in chromium exposed population, Sci. Total Environ. 430 (2012) 68–74. https://doi.org/10.1016/j.scitotenv.2012.04.063.

[5] F. Wu, H. Sun, T. Kluz, H.A. Clancy, K. Kiok, M. Costa, Epigallocatechin-3-gallate (EGCG) protects against chromate-induced toxicity in vitro, Toxicol. Appl. Pharmacol. 258 (2012) 166–175. https://doi.org/10.1016/j.taap.2011.10.018.

[6] K.P. Nickens, S.R. Patierno, S. Ceryak, Chromium genotoxicity: A double-edged sword, Chem. Biol. Interact. 188 (2010) 276–288. https://doi.org/10.1016/j.cbi.2010.04.018.

[7] C.M. Thompson, C.R. Kirman, D.M. Proctor, L.C. Haws, M. Suh, et al., A chronic oral reference dose for hexavalent chromium-induced intestinal cancer, J. Appl. Toxicol. 34 (2014) 525–536. https://doi.org/10.1002/jat.2907.

[8] A. Seidler, S. Jähnichen, J. Hegewald, A. Fishta, O. Krug, et al., Systematic review and quantification of respiratory cancer risk for occupational exposure to hexavalent chromium, Int. Arch. Occup. Environ. Health. 86 (2013) 943–955. https://doi.org/10.1007/s00420-012-0822-0.

[9] Y. Mu, H. Wu, Z. Ai, Negative impact of oxygen molecular activation on Cr(VI) removal with core–shell Fe@Fe2O3 nanowires, J. Hazard. Mater. 298 (2015) 1–10. https://doi.org/10.1016/j.jhazmat.2015.05.008.

[10] M.K. Michailides, A.G. Tekerlekopoulou, C.S. Akratos, S. Coles, S. Pavlou, D.V. Vayenas, Molasses as an efficient low-cost carbon source for biological Cr(VI) removal, J. Hazard. Mater. 281 (2015) 95–105. https://doi.org/10.1016/j.jhazmat.2014.08.004.

[11] K. StĘpniewska, Z. Bucior, Chromiumcontamination of Soils, Waters, and Plants in the Vicinity of a Tannerywaste Lagoon, Environ. Geochem. Health. 23 (2001) 241–245. https://doi.org/10.1023/A:1012247230682.

[12] D. Kumar, S.P. Gangwar, Role of antioxidants in detoxification of Cr (VI) toxicity in laboratory rats, J. Environ. Sci. Eng. 54 (2012) 441–446.

[13] F.C. Manning, L.J. Blankenship, J.P. Wise, J. Xu, L.C. Bridgewater, S.R. Patierno, Induction of internucleosomal DNA fragmentation by carcinogenic chromate: relationship to DNA damage, genotoxicity, and inhibition of macromolecular synthesis, Environ. Health Perspect. 102 (1994) 159–167. https://doi.org/10.1289/ehp.94102s3159.

[14] X.-H. Zhang, X. Zhang, X.-C. Wang, L.-F. Jin, Z.-P. Yang, et al., Chronic occupational exposure to hexavalent chromium causes DNA damage in electroplating workers, BMC Public Health. 11 (2011) 224. https://doi.org/10.1186/1471-2458-11-224.

[15] A. Kortenkamp, M. Casadevall, S.P. Faux, A. Jenner, R.O.J. Shayer, et al., A Role for Molecular Oxygen in the Formation of DNA Damage during the Reduction of the Carcinogen Chromium(VI) by Glutathione, Arch. Biochem. Biophys. 329 (1996) 199–207. https://doi.org/10.1006/abbi.1996.0209.

[16] L. Cheng, S. Liu, K. Dixon, Analysis of repair and mutagenesis of chromium-induced DNA damage in yeast, mammalian cells, and transgenic mice, Environ. Health Perspect. 106 (1998) 1027–1032. https://doi.org/10.1289/ehp.98106s41027.

[17] J.F. Cerveira, M. Sánchez-Aragó, A.M. Urbano, J.M. Cuezva, Short-term exposure of nontumorigenic human bronchial epithelial cells to carcinogenic chromium(VI) compromises their respiratory capacity and alters their bioenergetic signature, FEBS Open Bio. 4 (2014) 594–601. https://doi.org/10.1016/j.fob.2014.06.006.

[18] T. O'Brien, Complexities of chromium carcinogenesis: role of cellular response, repair and recovery mechanisms, Mutat. Res. Mol. Mech. Mutagen. 533 (2003) 3–36. https://doi.org/10.1016/j.mrfmmm.2003.09.006.

[19] J.P. Wise, S.S. Wise, J.E. Little, The cytotoxicity and genotoxicity of particulate and soluble hexavalent chromium in human lung cells, Mutat. Res. Toxicol. Environ. Mutagen. 517 (2002) 221–229. https://doi.org/10.1016/S1383-5718(02)00071-2.

[20] D.M. Proctor, M. Suh, S.L. Campleman, C.M. Thompson, Assessment of the mode of action for hexavalent chromium-induced lung cancer following inhalation exposures, Toxicology. 325 (2014) 160–179. https://doi.org/10.1016/j.tox.2014.08.009.

[21] K. Straif, L. Benbrahim-Tallaa, R. Baan, Y. Grosse, B. Secretan, et al., A review of human carcinogens—Part C: metals, arsenic, dusts, and fibres, Lancet Oncol. 10 (2009) 453–454. https://doi.org/10.1016/S1470-2045(09)70134-2.

[22] L.M. Beaver, E.J. Stemmy, A.M. Schwartz, J.M. Damsker, S.L. Constant, et al., Lung Inflammation, Injury, and Proliferative Response after Repetitive Particulate Hexavalent Chromium Exposure, Environ. Health Perspect. 117 (2009) 1896–1902. https://doi.org/10.1289/ehp.0900715.
[23] J.M. Cullen, J.M. Ward, C.M. Thompson, Reevaluation and Classification of Duodenal Lesions in B6C3F1 Mice and F344 Rats from 4 Studies of Hexavalent Chromium in Drinking Water, Toxicol. Pathol. 44 (2016) 279–289. https://doi.org/10.1177/0192623315611501.
[24] Y. Wang, H. Su, Y. Gu, X. Song, J. Zhao, Carcinogenicity of chromium and chemoprevention: a brief update, Onco. Targets. Ther. 10 (2017) 4065–4079. https://doi.org/10.2147/OTT.S139262.
[25] J. Yang, M. Yu, W. Chen, Adsorption of hexavalent chromium from aqueous solution by activated carbon prepared from longan seed: Kinetics, equilibrium and thermodynamics, J. Ind. Eng. Chem. 21 (2015) 414–422. https://doi.org/10.1016/j.jiec.2014.02.054.
[26] S. Sugashini, K.M.M.S. Begum, Preparation of activated carbon from carbonized rice husk by ozone activation for Cr(VI) removal, New Carbon Mater. 30 (2015) 252–261. https://doi.org/10.1016/S1872-5805(15)60190-1.
[27] S.E. Bailey, T.J. Olin, R.M. Bricka, D.D. Adrian, A review of potentially low-cost sorbents for heavy metals, Water Res. 33 (1999) 2469–2479. https://doi.org/10.1016/S0043-1354(98)00475-8.
[28] S. Salahi, T. Ghaffari, Antibacterial efficacy of green-synthesized silver nanoparticles from rosemary, pennyroyal, and eucalyptus extracts against E. coli and S. aureus bacteria, Synth. Sinter. 4 (2024) 101–107. https://doi.org/10.53063/synsint.2024.42218.
[29] P. Elliott, S. Ragusa, D. Catcheside, Growth of sulfate-reducing bacteria under acidic conditions in an upflow anaerobic bioreactor as a treatment system for acid mine drainage, Water Res. 32 (1998) 3724–3730. https://doi.org/10.1016/S0043-1354(98)00144-4.
[30] G.W. Staples, Revision of Asiatic Poraneae (Convolvulaceae) – Cordisepalum, Dinetus, Duperreya, Porana, Poranopsis , and Tridynamia, Blumea - Biodiversity, Evol. Biogeogr. Plants. 51 (2006) 403–491. https://doi.org/10.3767/000651906X622067.
[31] G.W. Staples, D.F. Austin, Revision of Neptropical Calycobolus and Porana (Convolvulaceae), Edinburgh J. Bot. 66 (2009) 133–153. https://doi.org/10.1017/S0960428609005319.
[32] G. Chen, Y. Lu, M. Yang, J. Li, B. Fan, Medicinal uses, pharmacology, and phytochemistry of Convolvulaceae plants with central nervous system efficacies: A systematic review, Phyther. Res. 32 (2018) 823–864. https://doi.org/10.1002/ptr.6031.
[33] S. Nacef, H. Ben Jannet, P. Abreu, Z. Mighri, Phenolic constituents of Convolvulus dorycnium L. flowers, Phytochem. Lett. 3 (2010) 66–69. https://doi.org/10.1016/j.phytol.2009.12.001.
[34] D.F. Austin, Evolvulus alsinoides (Convolvulaceae): An American herb in the Old World, J. Ethnopharmacol. 117 (2008) 185–198. https://doi.org/10.1016/j.jep.2008.01.038.
[35] M. Ranjbar, A. Ezazi, F. Ghahremaninejad, Taxonomic notes on Convolvulus sect. Serospinescentes (Convolvulaceae), Feddes Repert. 128 (2017) 17–35. https://doi.org/10.1002/fedr.201600020.
[36] N.M. Al-Enazi, Phytochemical screening and biological activities of some species of alpinia and Convolvulus plants, Int. J. Pharmacol. 14 (2018) 301–309. https://doi.org/10.3923/ijp.2018.301.309.
[37] B. Salehi, B. Krochmal-Marczak, D. Skiba, J.K. Patra, S.K. Das, et al., Convolvulus plant—A comprehensive review from phytochemical composition to pharmacy, Phyther. Res. 34 (2020) 315–328. https://doi.org/10.1002/ptr.6540.
[38] I. Mindru, G. Marinescu, D. Gingasu, L. Patron, C. Ghica, M. Giurginca, Blue CoAl2O4 spinel via complexation method, Mater. Chem. Phys. 122 (2010) 491–497. https://doi.org/10.1016/j.matchemphys.2010.03.032.
[39] Li, Z.F. Yan, G.Q. Lu, Z.H. Zhu, Synthesis and Structure Characterization of Chromium Oxide Prepared by Solid Thermal Decomposition Reaction, J. Phys. Chem. B. 110 (2006) 178–183. https://doi.org/10.1021/jp053810b.
[40] K.H. Büchel, H. Moretto, P. Woditsch, Industrial Inorganic Chemistry, Wiley. (2000). https://doi.org/10.1002/9783527613328.
[41] M. Ocaña, Nanosized Cr2O3 hydrate spherical particles prepared by the urea method, J. Eur. Ceram. Soc. 21 (2001) 931–939. https://doi.org/10.1016/S0955-2219(00)00288-0.
[42] A.C. Santulli, M. Feygenson, F.E. Camino, M.C. Aronson, S.S. Wong, Synthesis and Characterization of One-Dimensional Cr 2 O 3 Nanostructures, Chem. Mater. 23 (2011) 1000–1008. https://doi.org/10.1021/cm102930z.
[43] S. Sangeetha, R. Basha, K.J. Sreeram, S.N. Sangilimuthu, B. Unni Nair, Functional pigments from chromium(III) oxide nanoparticles, Dye. Pigment. 94 (2012) 548–552. https://doi.org/10.1016/j.dyepig.2012.03.019.
[44] K. AL-Rashedi, M. Farooqui, G. Rabbani, Characterizing Crystalline Chromium oxide Thin Film Growth by Sol-gel method on Glass Substrates, Orient. J. Chem. 34 (2018) 2203–2207. https://doi.org/10.13005/ojc/3404064.
[45] T. Rajkumar, G. Ranga Rao, Synthesis and characterization of hybrid molecular material prepared by ionic liquid and silicotungstic acid, Mater. Chem. Phys. 112 (2008) 853–857. https://doi.org/10.1016/j.matchemphys.2008.06.046.
[46] Rakesh, S. Ananda, N.M.M. Gowda, Synthesis of Chromium(III) Oxide Nanoparticles by Electrochemical Method and Mukia Maderaspatana Plant Extract, Characterization, KMnO Decomposition and Antibacterial Study, Mod. Res. Catal. 02 (2013) 127–135. https://doi.org/10.4236/mrc.2013.24018.
[47] Y. Guo, N. Zhao, T. Zhang, H. Gong, H. Ma, et al., Compatibility and thermal decomposition mechanism of nitrocellulose/Cr 2 O 3 nanoparticles studied using DSC and TG-FTIR, RSC Adv. 9 (2019) 3927–3937. https://doi.org/10.1039/C8RA09632E.
[48] M.M. Abdullah, F.M. Rajab, S.M. Al-Abbas, Structural and optical characterization of Cr2O3 nanostructures: Evaluation of its dielectric properties, AIP Adv. 4 (2014) 027121. https://doi.org/10.1063/1.4867012.
[49] B.B. Kamble, M. Naikwade, K.M. Garadkar, R.B. Mane, K.K.K. Sharma, et al., Ionic liquid assisted synthesis of chromium oxide (Cr2O3) nanoparticles and their application in glucose sensing, J. Mater. Sci. Mater. Electron. 30 (2019) 13984–13993. https://doi.org/10.1007/s10854-019-01748-5.
[50] T. Ivanova, K. Gesheva, A. Cziraki, A. Szekeres, E. Vlaikova, Structural transformations and their relation to the optoelectronic properties of chromium oxide thin films, J. Phys. Conf. Ser. 113 (2008) 012030. https://doi.org/10.1088/1742-6596/113/1/012030.
[51] T.I. Alanazi, R.A. Alenazi, A.M. El Sayed, Tuning the band gap, optical, mechanical, and electrical features of a bio-blend by Cr2O3/V2O5 nanofillers for optoelectronics and energy applications, Sci. Rep. 14 (2024) 12537. https://doi.org/10.1038/s41598-024-62643-6.
[52] M.G. Tsegay, H.G. Gebretinsae, G.G. Welegergs, S. Azizi, M.P. Seopela, et al., Optical response of green synthesized thin Cr2O3 films prepared via drop and spin coatings, Mater. Today Proc. (2023). https://doi.org/10.1016/j.matpr.2023.06.225.
[53] J. Singh, V. Verma, R. Kumar, S. Sharma, R. Kumar, Effect of structural and thermal disorder on the optical band gap energy of Cr2O3 nanoparticles, Mater. Res. Express. 6 (2019) 085039. https://doi.org/10.1088/2053-1591/ab195c.
[54] G. Singh, D. Jalandhara, K. Yadav, Effect of grain size on optical properties of iron oxide nanoparticles, API Conf. Proc. 1728 (2016) 020409. https://doi.org/10.1063/1.4946460.